Relaxation times of Arctic mixed-phase clouds to short-term aerosol perturbations under different surface forcings

Gesa K. Eirund[1], Anna Possner[2], and Ulrike Lohmann[1]

[1]Institute for Atmospheric and Climate Sciences, ETH Zurich, Zurich, Switzerland
[2]Department of Global Ecology, Carnegie Institution for Science, Stanford, California, USA

Correspondence to: Gesa K. Eirund (gesa.eirund@env.ethz.ch)

Abstract. The formation and persistence of low lying mixed-phase clouds (MPCs) in the Arctic depends on a multitude of processes, such as surface conditions, the environmental state, air mass advection and the ambient aerosol concentration. In this study, we focus on the relative importance of different aerosol perturbations (cloud condensation nuclei and ice nucleating particles; CCN and INP, respectively) on MPC properties in the central Arctic. To address this topic, we performed

5   high resolution large eddy simulations (LES) using the COSMO model and designed a case study for the Aerosol-Cloud Coupling and Climate Interactions in the Arctic (ACCACIA) campaign in March 2013. Motivated by ongoing sea ice retreat, we additionally contrast the simulated MPC that formed over an open ocean surface and a sea ice surface. We find that surface conditions highly impact cloud dynamics: over sea ice, a rather homogeneous, optically thin, mixed-phase stratus cloud forms. In contrast, the MPC over the open ocean has a stratocumulus-like cloud structure. With cumuli feeding moisture into the

10   stratus layer, the cloud features a higher liquid (LWC) and ice water content (IWC) and has a lifted cloud base compared to the cloud over sea ice.

Furthermore, we analyzed the aerosol impact on these two dynamically different regimes. Perturbations in the INP concentration increase the IWC and decrease the LWC consistently in both regimes. The cloud microphysical response to potential CCN perturbations occurs faster in the stratocumulus regime over the ocean, where the increased moisture flux favors rapid cloud

15   droplet formation and growth, leading to an increase in LWC following the aerosol injection. In addition, the IWC increases through increased immersion freezing and subsequent growth by deposition. Over sea ice, the maximum response is delayed by a factor of 2.5 compared to open ocean surface. However, independent of the cloud regime and aerosol perturbation, the cloud regains its original state after at most 12 h for an aerosol perturbation of 1000 cm^{-3}. Cloud microphysical and macrophysical peoperties relax to their unperturbed range, and any aerosol perturbation is efficiently buffered. A substantial fraction of the

20   aerosol is transported out of the boundary layer into the capping inversion, where the supersaturation is insufficient for aerosol activation. Our results are robust across different temperature ranges and insensitive to the aerosol injection period. Based on these results we postulate an efficient aerosol processing and transport mechanism that appears to inhibit any long-term aerosol impact on Arctic MPC properties.

1 Introduction

Clouds play a crucial role in the hydrological cycle and the radiative balance of the Earth-atmosphere system. However, clouds still comprise high uncertainties and their behavior under climate change scenarios is not yet well-understood. Hence, the magnitude of the cloud radiative forcing in the upcoming years remains unclear (IPCC, 2013). Mixed-phase clouds (MPCs)

5 contain both phases, i.e. ice and water, and are suggested to impact the radiative balance and climate sensitivity (Tan et al., 2016). MPCs occur either in mountainous terrain (Lohmann et al., 2016), or in cold regions of the planet, i.e. in high latitudes (Morrison et al., 2011). In the Arctic, MPCs occur approximately 40% of the time (Shupe et al., 2006) and are often observed as persistent low clouds (Shupe et al., 2011). Their radiative forcing at the surface is still ambiguous and determined in part by the distinct seasonal cycle at high latitudes. In summer, the reflection of incoming radiation dominates, while during the rest

10 of the year absorption and emission of longwave (LW) radiation prevails, potentially causing a warming effect at the surface (Curry et al., 1996). In recent years the Arctic has been warming at a faster rate than the rest of the globe (Serreze and Barry, 2011). As changes in the Arctic can impact mid latitude weather conditions, the climate state of the Arctic is important not only regionally but also hemisphere-wide (Cohen et al., 2014; Ye et al., 2018). As part of the climate system, MPC properties can be modified through changes in the Arctic climate and can at the same time impact their environment through radiative

15 effects (e.g. Bennartz et al., 2013; Van Tricht et al., 2016), eventually accelerating the current high latitude warming.

Arctic MPC amount and phase partitioning are governed by a multitude of processes operating in conjunction across a wide range of spatial scales; such as the large-scale dynamical forcing, surface processes, as well as the ambient aerosol concentration. The large-scale dynamical forcing determines air mass and hence water vapor advection, which is found to be crucial for the persistence of Arctic MPC (Morrison et al., 2011; Sedlar et al., 2012; Loewe et al., 2017). With ongoing sea

20 ice loss and the possibility of an ice-free Arctic by mid century (Overland and Wang, 2013), the impact of surface conditions on Arctic MPC has gained increasing attention over recent years (e.g. Schweiger et al., 2008; Palm et al., 2010; Vavrus et al., 2010; Liu et al., 2012; Sotiropoulou et al., 2016; Young et al., 2016). On the one hand, a more exposed open ocean surface has potential implications for cloud dynamics. Schweiger et al. (2008) using the 40-yr ECMWF Re-Analysis (ERA-40) product demonstrated that sea ice loss increased boundary layer height and led to more midlevel clouds. In addition, Sotiropoulou

25 et al. (2016) found increased stratocumulus or cumulus cloud formation over the ocean in contrast to thin stratus clouds over sea ice in observations from the Arctic Clouds in Summer Experiment (ACSE) campaign. A study by Young et al. (2016), specifically targeted at investigating cloud changes in the transition between open ocean and sea ice during the Aerosol-Cloud Coupling And Climate Interactions in the Arctic (ACCACIA) campaign, could support changes in cloud height over the ocean and besides reported fewer and larger cloud droplets as well as increased precipitation rates over the open ocean.

30 On the other hand, with more exposed open ocean surfaces, aerosol emissions may increase (Struthers et al., 2011; Browse et al., 2014; Gilgen et al., 2018) which could impact the cloud microphysics. With decreasing sea ice, trans-Arctic shipping is also projected to increase, exerting local aerosol perturbations (Khon et al., 2010; Peters et al., 2011). As suggested in a modeling study by Gilgen et al. (2018), sea salt and dimethyl sulfide emissions may dominate ship emissions in terms of cloud and radiation modification. Since the Arctic is a pristine environment, these aerosol perturbations could significantly impact

MPC formation and persistence. A reduction in the ambient cloud condensation nuclei (CCN) and hence cloud droplet number concentration (N_{drop}) can lead to cloud dissipation (Mauritsen et al., 2011; Loewe et al., 2017; Stevens et al., 2018) and/or changes in cloud liquid and ice water content (LWC and IWC, respectively) as could been seen in the studies of Christensen et al. (2014) and Possner et al. (2017). While several studies have investigated the response of MPCs to increased levels of

5 background CCN (e.g. Loewe et al., 2017; Young et al., 2017a; Stevens et al., 2018), the question whether temporary concentrated aerosol perturbations may affect the cloud thermodynamic or cloud-dynamic state for a prolonged time period remains unclear. Also disentangling the competing effects of environmental conditions and aerosol disturbances appears challenging (Jackson et al., 2012). In the past, Stevens and Feingold (2009) argued for a buffered aerosol response in certain cloud regimes. For mid-latitude convective clouds, Miltenberger et al. (2018) showed that cloud fraction is not impacted by aerosol perturba-

10 tions, but that aerosols may affect the organization of cloud pockets with larger, less widespread and more densely packed cells under levels of increased pollution. In simulations of trade winds shallow cumulus by Seifert et al. (2015) an initial aerosol response is seen, with an increased number of cumulus structures and decreased precipitation. Yet the system efficiently returns to an organized cloud structure in a quasi-stationary state after some hours, which is insensitive to the background aerosol concentration. Turbulent mixing of aerosols out of the polluted regions could potentially also dilute the aerosol concentration

15 and decrease the long-term aerosol response, as shown by Berner et al. (2015) in large eddy simulations (LES) of ship tracks in the Monterey Bay, or recently by Solomon et al. (2018) for MPCs over Oliktok Point, Alaska.

Here, we assess how these processing time-scales may differ for different cloud regimes of Arctic MPCs. For that purpose we perform high-resolution idealized LES to resolve the multitude of boundary layer processes that impact the cloud state. We contrast our results for different surface conditions (i.e. open ocean surface versus sea ice). To further address the robustness of

20 our results, we apply different perturbations across a ± 2 K temperature range and perform one simulation with a longer aerosol injection period. To validate our simulations we use observations obtained during the recent ACCACIA campaign (Lloyd et al., 2015; Young et al., 2016) in the European Arctic.

2 Model description and setup

LES are performed with the Consortium for Small-scale Modeling (COSMO) model in its configuration for idealized LES

25 experiments (Schättler et al., 2000). COSMO-LES has been proven to simulate MPCs in the Arctic with reasonable accuracy (Possner et al., 2017). Here, we simulate a single-layer stratocumulus case during the ACCACIA campaign on March 23rd, 2013. The simulations are initialized with the dropsonde profile number 5 released during the campaign. The obtained profiles are smoothed to exclude small-scale variability from the measurements as model input. In addition, the water vapor mixing ratio (q_v) was increased by 20% to account for the dry bias in dropsonde data (Ralph et al., 2005). The domain covers a 19.2

30 x 19.2 km large area around the location of dropsonde number 5. The horizontal resolution is 120 m, the vertical resolution is variable and specified with 20 to 25 m within the entire boundary layer and coarser resolution above cloud top. Radiation is treated interactively according to the Ritter and Geleyn (1992) radiation scheme and includes a diurnal cycle. The cloud microphysical tendencies are parameterized following the Seifert and Beheng (2006) two-moment scheme. As in Possner et al.

(2017) we use a prognostic treatment of ice nucleating particles (INP) and aerosols available for CCN activation. Cloud droplet activation is calculated according to Kohler theory (Nenes and Seinfeld, 2003). CCN are advected throughout the domain, are depleted by cloud droplet formation and precipitation, and are released through evaporation. Throughout the simulations the CCN composition is assumed to be ammoniumbisulfate. Prognostic INPs are treated as in Solomon et al. (2015). This scheme

5 parameterizes immersion freezing following the DeMott et al. (2015) temperature dependence and captures the depletion and replenishment of INPs.

We initialize the simulations with two background modes of potential CCN which comprise a larger mode (1.3 μm) and a smaller mode (0.2 μm). The number concentrations were chosen according to observations from the Passive Cavity Aerosol Spectrometer Probe over the ocean at low altitudes (Young et al., 2016), with concentrations of 0.54 cm^{-3} and 48.3 cm^{-3} for

10 the larger and smaller mode, respectively. INP were initialized with a concentration of 3.3 L^{-1}, which is within the range of predicted ice crystal number concentrations (N_{ice}) by different parameterizations in Young et al. (2016).

We performed control simulations over sea ice and open ocean and evaluated these against available observations. The simulations were initialized with the same atmospheric profile. For the sea ice case, the COSMO sea ice model (Mironov et al., 2012) was switched on. To exclude influences from variable turbulent fluxes, the sensible and latent heat flux were set to 25 and

15 23 W m^{-2} over ocean and to 1 and 0.8 W m^{-2} over sea ice, which is within the observed range (Young et al., 2016). Surface roughness length was assumed to be higher over the ocean with 0.0002 m in contrast to 0.0001 m over sea ice. Divergence was prescribed at the surface. The divergence was relaxed linearly to $4 * 10^{-6}$ s^{-1} at the inversion height and kept constant above. To compensate for the subsidence heating, we included negative horizontal advective temperature tendencies, while all other tendencies were set to zero to prevent any influence of boundary layer moistening or drying by large-scale advection.

20 ## 2.1 Model perturbation experiments

In order to study the effects of aerosol perturbations, an additional mode of potential CCN or INP was released at every grid point and vertical level once the surface precipitation stabilized at 1.5 h following initialization. The perturbation mode was assumed to be slightly smaller than the background modes (0.19 μm) and to have the same chemical composition as the background modes. As well as the background aerosols, the aerosol perturbations are prognostic and can change over time.

25 Perturbation aerosol concentrations relevant for CCN activation were increased successively by a factor of 2 from 100 to 1000 cm^{-3}. For INP perturbations we doubled the background concentration and increased the INP by a factor of 3. A summary of all performed simulations is found in Table 1.

Given the pronounced sensitivity of ice-phase processes to atmospheric temperature, we test the robustness of our results across a ± 2 K temperature range in the background state. In these experiments the entire initial temperature profile was shifted

30 towards colder or warmer temperatures at constant relative humidity. Finally, we altered the time period over which the aerosol perturbation was applied. While in most simulations the aerosol perturbation was injected within a single time step and freely evolved from there, the same amount of aerosol was injected over 0.5 hours in simulation *1000CCN_0.5h*.

Name	CCN (cm^{-3})	CCN perturb (cm^{-3})	INP (L^{-1})	INP perturb (L^{-1})	T perturb (K)
control	48.84	-	3.3	-	-
100CCN	48.84	100	3.3	-	-
200CCN	48.84	200	3.3	-	-
500CCN	48.84	500	3.3	-	-
1000CCN	48.84	1000	3.3	-	-
1000CCN_0.5h	48.84	$\sum$1000	3.3	-	-
3INP	48.84	-	3.3	3	-
10INP	48.84	-	3.3	10	-
control_+2K	48.84	-	3.3	-	+2
control_-2K	48.84	-	3.3	-	-2
1000CCN_+2K	48.84	1000	3.3	-	+2
1000CCN_-2K	48.84	1000	3.3	-	-2
10INP_+2K	48.84	-	3.3	10	+2
10INP_-2K	48.84	-	3.3	10	-2

Table 1. Summary of all experiments performed. All settings listed here were run over an open ocean and sea ice surface, except *1000CCN_0.5h*, which was performed over open ocean only.

3   Evaluation of background state

Our simulated case is characterized by a strong inversion at a height of 1.2 km, capping the single cloud layer below (Fig. 1). The boundary layer in both control simulations is stably stratified, as seen in the positive gradient in the ice-liquid potential temperature (θ_{il}) and the negative gradient in the total water content (q$_t$) in Fig. 1. Over the ocean surface an unstable surface

5   layer forms due to the non-zero surface fluxes. The remainder of the boundary layer is stably stratified, which prevents the formation of a mixed boundary layer.

Our model successfully simulates a liquid-topped MPC with ice sedimenting out of the liquid layer in both control simulations, according to observations. We summarize the simulated mean cloud properties of the unperturbed simulations in Table 2. The mean N_{ice} of 0.19 L^{-1} in *ocean_control* is lower in our model simulations. However, the observed variability of N_{ice} is

10   exceptionally high due to a crystal fragmentation event at cloud base (Young et al., 2016), such that we consider our simulated values to be within the observed range. N_{drop} is underestimated in our model simulations as compared to observations. The low bias in N_{drop} is attributed to low CCN concentrations in the boundary layer, which has been found to result from cloud and boundary layer dynamics. A strong net upward vertical transport at cloud top leads to an accumulation of aerosols in the inversion layer (Fig. 2) where they remain and do not activate. Cloud top turbulence is found to be insufficient to re-entrain the

15   aerosol into the boundary layer where they would activate and act as CCN. In a dry run, where the boundary layer was forced to remain sub-saturated, this phenomenon does not take place. As a result, the low CCN concentration of <10 cm^{-3} within the boundary layer leads to in-cloud N_{drop} values of 3-4 cm^{-3}, whereas at cloud top N_{drop} reaches 10 cm^{-3} due to entrainment
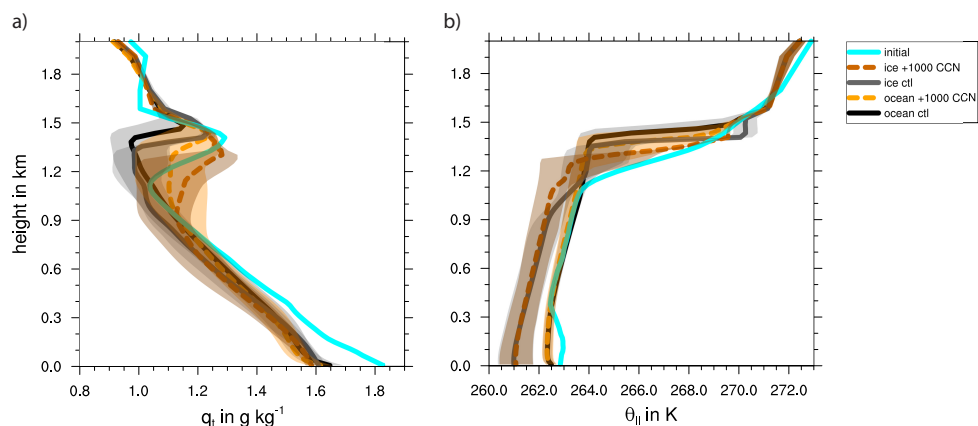
Figure 1. Total median and interquartile ranges of the a) total water content q_t ($q_t = q_c + q_v + q_i$) and b) the ice-liquid potential temperature θ_{il} in the *ocean_control* and *ice_control* simulations as well as the most perturbed *1000CCN* simulations. The blue lines represent the initial profiles.

	Cloud extend (m)	LWMR (g kg^{-1})	N_{drop} (cm^{-3})	N_{ice} (L^{-1})	R_{drop} (μm)	R_{ice} (μm)
Observations ocean	700-1500	0.24±0.13	63±30	0.55±0.95	10	-
ocean_control	215-1486	0.11±0.04	3.99±0.94	0.17±0.04	12.01±1.03	14.15±2.31
Observations sea ice	300-700	0.05±0.04	110±36	0.47±0.86	5	-
ice_control	158-1386	0.05±0.01	3.39±0.81	0.06±0.02	10.54±0.90	15.0±3.40

Table 2. Vertically averaged (±1 std) cloud properties derived from the ACCACIA in-situ observations (Young et al., 2016, 2017b) and the *ocean_control* and *ice_control* simulation (as temporal mean from 1.5-16 h). The cloud extent in the model is calculated as the highest/lowest level, where q_c>0.01 g m^{-3}. Note that the airplane did not sample the lower and upper levels, hence we calculated the modeled averaged quantities only over the observed range (300-1500 m). As in the observations, all modeled quantities represent in-cloud values (q_c>0.01 g m^{-3} and q_i>0.0001 g m^{-3}).

of a few CCN from above. This vertical distribution of N_{drop} with a maximum at cloud top in combination with a pronounced in-cloud minimum, as also been simulated by Solomon et al. (2018) and therefore does not seem to be unique to our model or setup. Partly compensating for the lower N_{drop}, cloud droplets are 17% (*ocean_control*) and 47% (*ice_control*) larger in our simulations as compared to observations (Table 2).

4 Surface flux impact on cloud dynamics

The simulated effect of surface fluxes is illustrated in Fig. 3, showing a snapshot of the updraft velocity and LWP over ocean and sea ice. The different surface conditions yield two differing cloud regimes: over ocean, where surface fluxes are increased,
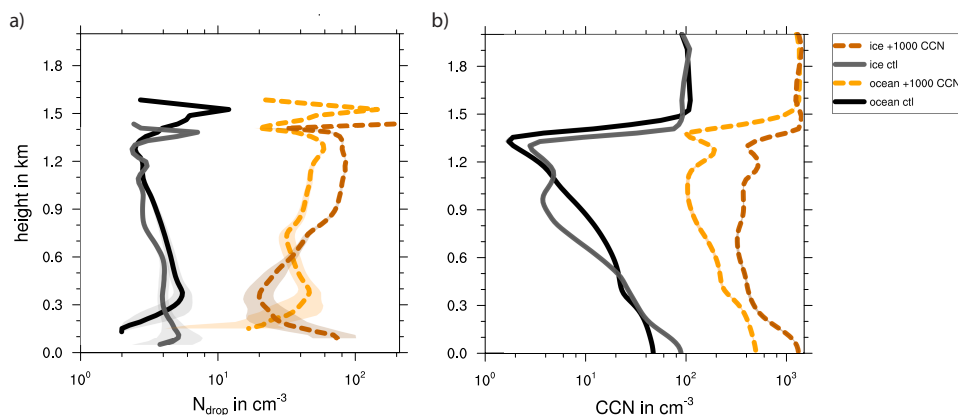
Figure 2. Temporal mean (1.5-16 h) and spatial median and interquartile ranges of the a) N_{drop} and b) the sum of all CCN tracers (i.e. background and perturbation mode) in the *ocean_control* and *ice_control* simulations as well as most perturbed *1000CCN* simulations.

the updrafts are higher, leading to cumulus towers detraining into the stratus deck and to a domain wide shallow stratocumulus cloud structure. Within the shallow cumuli the LWP increases up to 250 g m^{-2}, 5 times higher than in the surrounding stratus layer. In contrast, over sea ice the updrafts are low and a spatially homogeneous stratus forms. The LWP of the stratus cloud remains mainly below 50 g m^{-2}.

5   These dynamic differences feed back onto the vertical cloud extend (Fig. 4 and Table 2). Supported by the stronger updrafts, the cloud penetrates approximately 100 m deeper into the inversion layer and the cloud base is lifted by 100 m over the open ocean. These high updrafts and the increased moisture flux allow the droplets as well as the crystals to grow larger (Table 2) and initiate precipitation, which is increased over the ocean (on average 1.17 mm d^{-1} at the surface). Rain forms mainly in the updrafts where droplets can grow at a faster rate than in the surrounding stratus cloud. Over sea ice, low updrafts inhibit

10   a strong moisture flux throughout the boundary layer, resulting in a thinner cloud that is mainly confined to a layer of 200 m below the temperature inversion. Cloud droplets are smaller (Table 2) and precipitation formation is less efficient than over the open ocean (on average 0.58 mm d^{-1}).

Freezing processes in both simulations are determined by ice crystal growth by deposition throughout the cloud as well as immersion freezing occurring at cloud top where new ice crystals nucleate. Immersion freezing is more efficient over the open

15   ocean because more INP are available due to a higher cloud top and LW cooling is increased up to 3 K h^{-1} (Fig. 5). The more numerous ice crystals can then efficiently grow through deposition (Fig. S1), leading to a higher IWC over the ocean.
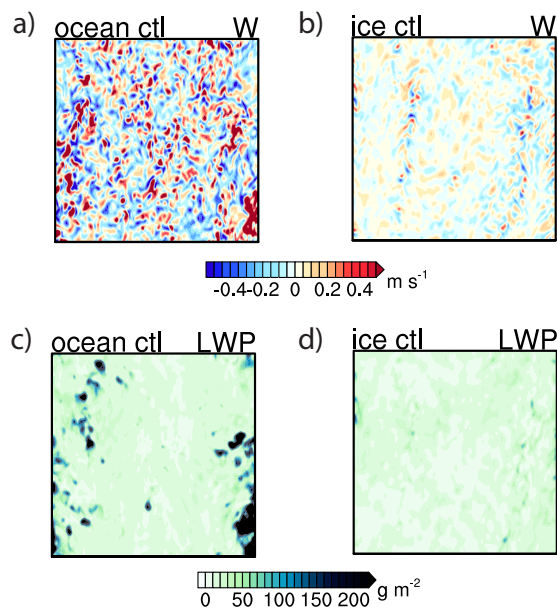
Figure 3. Temporal snapshot of a,b) updrafts in the lower part of the cloud (400 m) and c,d) LWP for the *ocean_control* (left) and the *ice_control* case (right).

Due to the distinct cloud dynamics in both regimes, the effect of the aerosol perturbations differs. In the following we present results from several sensitivity simulations, investigating the effect of additional potential CCN and INP perturbations across different temperature ranges and aerosol injection lengths on the two cloud regimes.
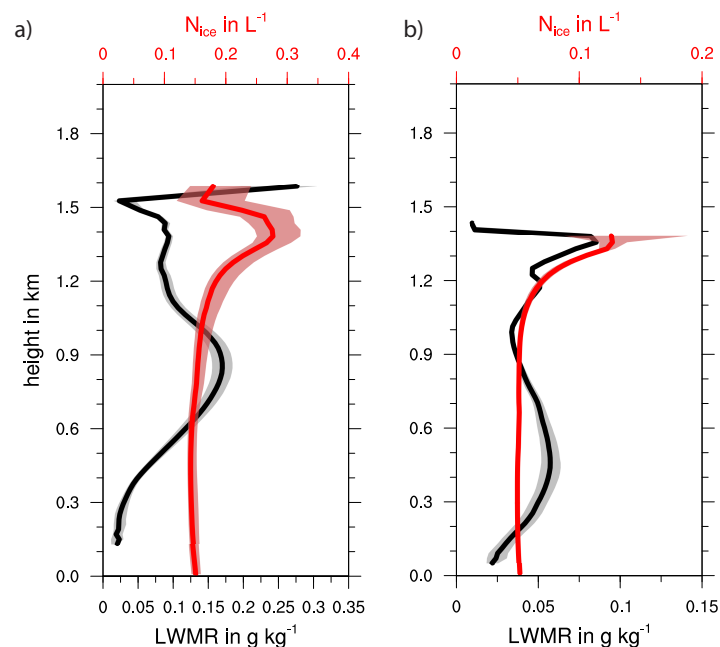
Figure 4. Temporal mean (1.5-16 h) and spatial median and inerquartile ranges of the N_{ice} (red) and LWMR (black) in the a) *ocean_control* and b) *ice_control* simulation. Only in-cloud values are plotted. Note the different axes for the *ice_control* simulation.

5 Robustness to perturbations in microphysics

5.1 Response to CCN perturbations

We performed simulations with potential CCN perturbations ranging from 100 to 1000 CCN cm^{-3}. The perturbations were applied (as described in section 2) following the strong precipitation event 1.5 h after initialization.

5 Over the ocean, the cloud responds almost immediately to CCN perturbations with an increase in LWP (Fig. 6a). A CCN perturbation of 500 CCN cm^{-3} is sufficient to significantly perturb the liquid cloud properties within the first hour upon seeding. By perturbing the cloud with 1000 CCN cm^{-3}, the LWP almost triples after 2 h. High CCN concentrations in combination with strong updrafts and an enhanced moisture flux allow fast additional droplet formation, which immediately increases the vertical mean N_{drop} from 3 to 163 cm^{-3} and decreases the cloud droplet radius (R_{drop}) from 11 to 3 μm in the *1000CCN* simulation

10 (Fig. S2 and S3), commonly known as the Twomey effect (Twomey, 1974). After subsequent droplet growth, the LWP reaches its peak 1.5-2.5 h upon seeding. Apart from changes in LWP, also N_{ice} and the IWP are affected by CCN perturbations. As suggested by Garrett and Zhao (2006), the strong vertical gradient of liquid water in the air column increases cloud top LW cooling (Fig. 5). This increased LW cooling rate (up to -3.6 K h^{-1}) leads on the one hand to additional cloud top turbulence and increased cloud top entrainment. On the other hand it triggers immersion freezing below the top cloud layer, leading to

15 an increased N_{ice} in the perturbed simulations (Fig. 6c and S4), as previously found by Possner et al. (2017). Additional ice
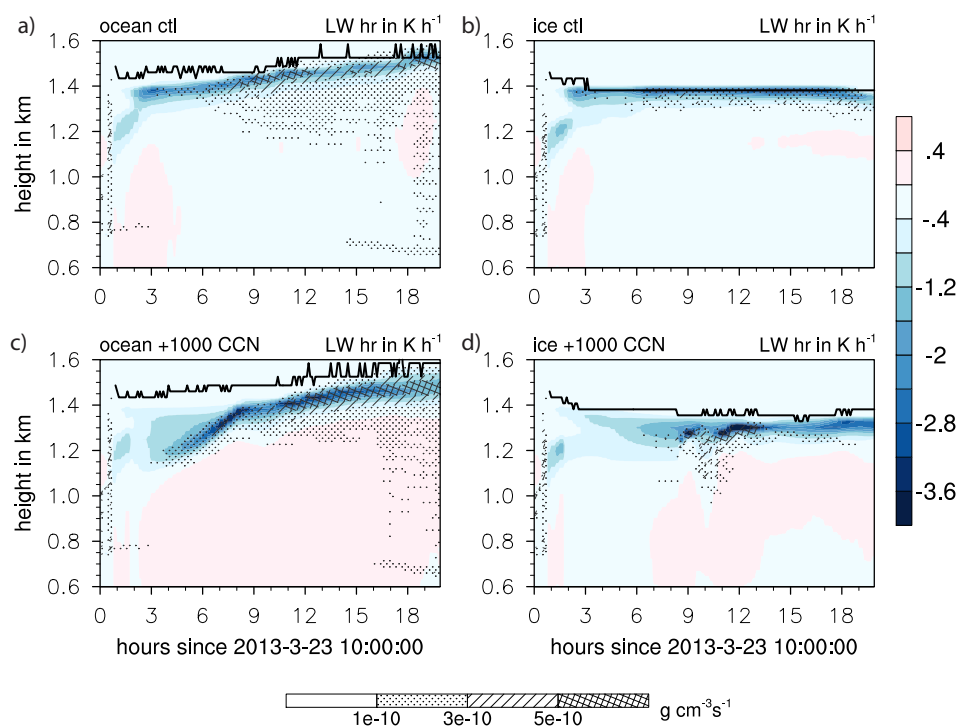
Figure 5. LW heating rate (color), immersion freezing rate (hatching) and cloud top of the uppermost cloud layer, where $q_c > 0.01\,\mathrm{g\,m^{-3}}$ are shown for the a) *ocean_control* and b) *ice_control* simulations and c,d) the respective *1000CCN* simulations.

crystal growth by deposition increases the total IWC (Fig. S1), which agrees well with results from Solomon et al. (2018). The relative importance of crystal growth by deposition versus immersion freezing in the most perturbed/unperturbed simulation is shown in Fig. 7. From hour 3-9 of the simulation, immersion freezing rates are increased in the perturbed simulation contributing to the initial IWP increase. With time, the additional IWP is a result of an increase in N_{ice} due to the entrainment of INP

5   through cloud deepening and colder temperatures at higher altitudes, and the subsequent growth of new N_{ice} by deposition. The cloud deepening in the simulations over the open ocean (as seen in Fig. 5a,c) is driven by the detrainment of moisture by overshooting cumulus towers until saturation above cloud-top is reached.

The initial effect of CCN perturbations strongly depends on the cloud regime. Due to the lower updrafts and the decreased moisture flux over sea ice, the increase in N_{drop} after the CCN injection is slower and cloud droplet growth limited (Fig. S2 and

10 S3). The response of the LWP to CCN perturbations also lasts longer and persists for up to 2-3 times as long as compared to the open ocean (Fig. 6b). The decreased spatial variability over sea ice leads to a significant change of the liquid cloud properties with a CCN perturbation of only 100 CCN cm^{-3}. After 7 h upon seeding, the maximum LWP increases to 150 g m^{-2} in the most perturbed simulation, exceeding the LWP in the *control* run by a factor of 5. The IWP and N_{ice} reach a maximum shortly
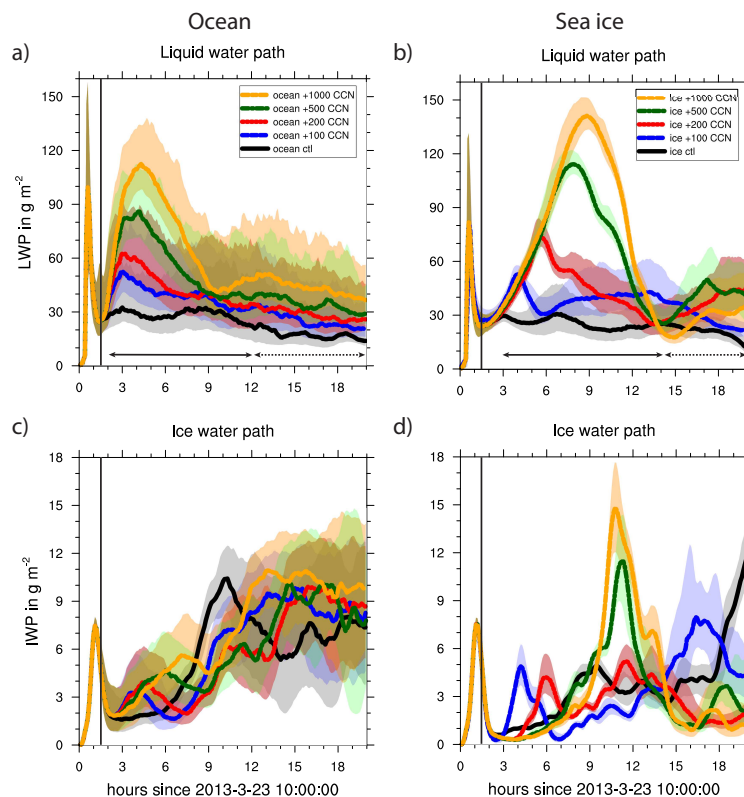
Figure 6. a,b) LWP and c,d) IWP over the open ocean (left) and sea ice (right) in the *control* run and all sensitivity simulations. The solid lines depict the median, the shading the interquartile ranges. The vertical black line indicates the CCN perturbation injection and the two arrows the polluted (solid arrow) and post-polluted (dashed arrow) periods used for averaging in Table 3.

after the maximum increase in LWP (Fig. 6d and S4). As over the ocean, increased LW cooling (up to -3.6 K h^{-1}) when the LWC at cloud top is highest, triggers immersion freezing in the upper 300 m of the cloud. Together with increased ice crystal growth by deposition, which is up to 6 times as high as compared to the control simulation, both freezing mechanisms lead to an increase in the ice phase and a pronounced peak in IWP following the LWP maximum.

5   As evident from Fig. 6, the elevated LWP decreases after reaching its maximum and approximates the LWP of the control simulation. Independent of the strength of the CCN perturbation, all simulations relax to their unperturbed state. Fig. 8 visualizes the spatio-temporal evolution of the LWP within the domain over the open ocean. In the first hours after the initiation of the perturbation the LWP throughout the domain and the number of cumuli within the stratus layer is increased (Fig. 8b). However, after 10 h the cloud organizes back to structures observed in the control simulation (Fig. 8a). This behavior is qualita-

10   tively similar to what had previously been observed in numerical aerosol-perturbed simulations of warm-phase shallow cumuli (Seifert et al., 2015). There, evaporative processes caused the limited sensitivity of the cloud field to aerosol perturbations. In our study, the main mechanism determining the diminished aerosol effect in both cloud regimes, is the vertical transport of
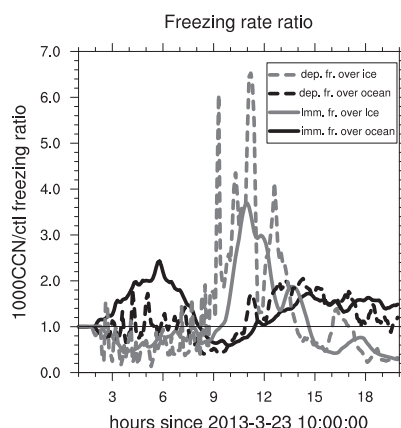
Figure 7. Ratio of immersion freezing and ice crystal growth by deposition between the most perturbed simulation (*1000CCN*) and the *ocean_control* and *ice_control* simulation, respectively.
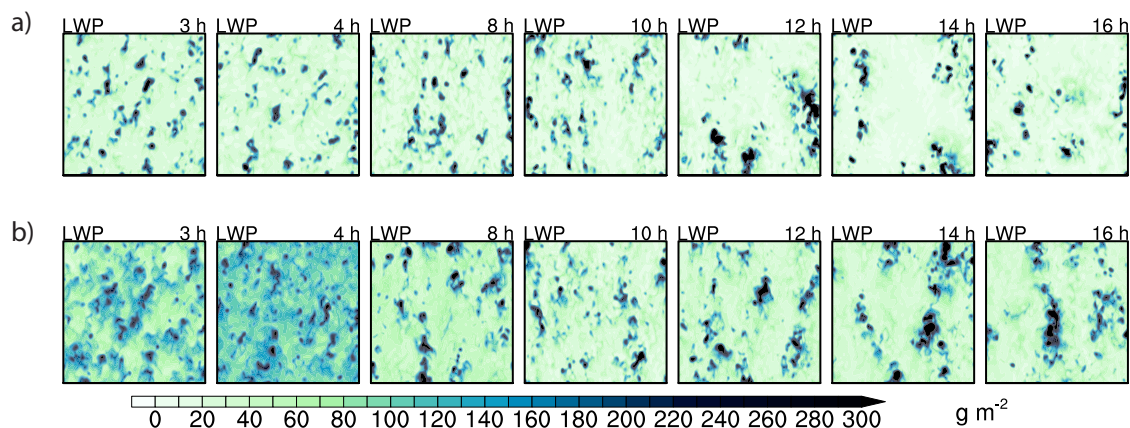
Figure 8. LWP for a) *ocean_control* and the b) open ocean *1000CCN* simulation.

additional aerosols out of the boundary layer (Fig. 2b). In both cloud regimes, aerosols get transported into the inversion layer, which acts as a mixing barrier and prevents the unactivated CCN from being depleted through cloud processing.

Note the different time scales of the cloud response to CCN perturbations. Over open ocean the return time to unperturbed conditions is approximately twice the injection-to-peak time, over sea ice the injection-to-peak time equals the return time. We suggest that the cloud regime does impact the maximum response as well as the response times, however, in the long-term, the effect of CCN does not significantly change the cloud mean state, independent of the cloud regime.

5.2 Response to INP perturbations

Similarly to CCN perturbations we applied two INP perturbations of 3 and 10 INP L^{-1} after 1.5 h simulation time. In both dynamic regimes the IWP increases and the LWP decreases with more available INP (Fig. 9). However, in neither regime does a perturbation of 10 INP L^{-1} glaciate the cloud and we still find a mixed-phase regime to be present after 20 h. This finding is consistent with other studies investigating cloud glaciation under INP perturbations (e.g. Solomon et al., 2018).

The stratus cloud over sea ice is initially more susceptible to INP perturbations than the open ocean stratocumulus cloud, with increased immersion freezing and growth by deposition immediately following the INP injection.
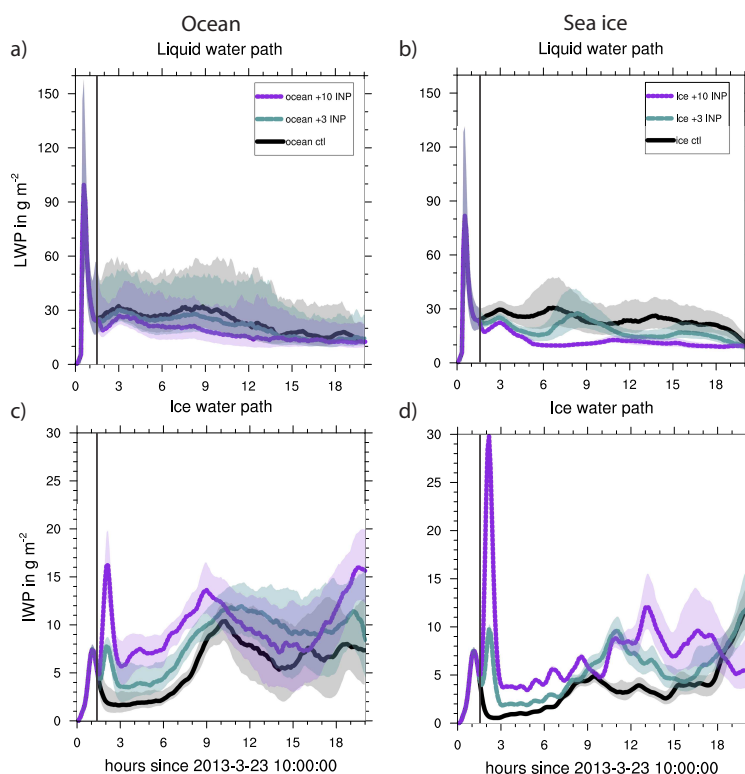
Figure 9. a,b) LWP and c,d) IWP over the open ocean (left) and sea ice (right) in the *control* run and all INP sensitivity simulations. The solid lines depict the median, the shading the interquartile ranges.

5.3 Invariance of results across temperature regimes

To address the robustness of our results from the perturbed simulations, we performed each the *control*, the *1000CCN*, and the *10INP* simulation over sea ice and open ocean in 2 K warmer and colder conditions, respectively.

As illustrated in Fig. 10, the cloud response as well as the response mechanism are invariant to a wide range of environmental conditions. Additionally, we can infer a temperature-dependent amplitude in the aerosol response. Fig. 10 shows that the aerosol response is subdued in a warmer environment, while in a colder environment ice-phase processes dominate and the IWP increases/LWP decreases. It is also worth noting that neither in the warmer nor in the colder simulation the cloud deepens.

5 Hence the IWP towards the end of the simulation relaxes back to its initial value and does not stay elevated as in the *1000CCN* case. In a colder environment ice-phase processes stabilize the cloud and prevent it from rising. In a warmer environment at constant relative humidity, the liquid water saturation above cloud requires a larger change in water vapor mixing ratio to reach saturation which prevents the cloud from deepening. Furthermore, the longer response time and larger sensitivity within more stratiform clouds over sea ice than more convective stratocumulus over the open ocean seems robust under different

10 temperature ranges.

For INP perturbations, the temperature change initiates increased freezing and a higher IWP for the colder simulation and vice versa for the warmer simulation. Determined by the nature of the DeMott et al. (2015) immersion freezing parameterization, more (less) INP activate at colder (warmer) temperatures (Fig, S5).
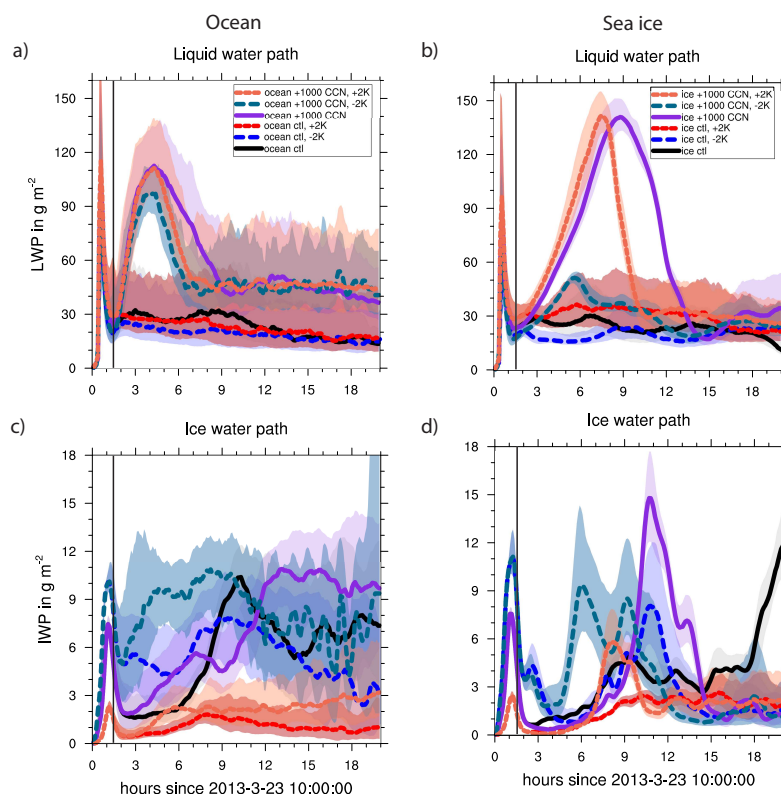
Figure 10. a,b) LWP and c,d) IWP over the open ocean (left) and sea ice (right) in the *control* run and the respective *1000CCN* simulations in their regular state and 2 K warmer and colder conditions. The solid lines depict the median, the shading the interquartile ranges.

5.4 Consistent response independent of perturbation injection period

Finally, we address the importance of the length of the aerosol injection period. Our perturbations experiments summarized in Table 2 and discussed in section 5.1-5.3 were performed representing a rapid increase in aerosol concentration within a single model time step.

5   To test whether our conclusions hold in perhaps more realistic conditions where aerosol concentrations increase gradually over time, we performed an additional simulation for the *1000CCN* setup. Here the aerosol concentration increased over 0.5 h such that the CCN emissions integrated to 1000 cm^{-3} over the injection time span. Such conditions could correspond to (i) a cloud in contact with a polluted air mass, or (ii) a local source of a ship passing.

    The simulation shows that there is no change in response with respect to aerosol injection duration on these time scales (Fig.
10   11). Therefore, our conclusions remain valid for such conditions.
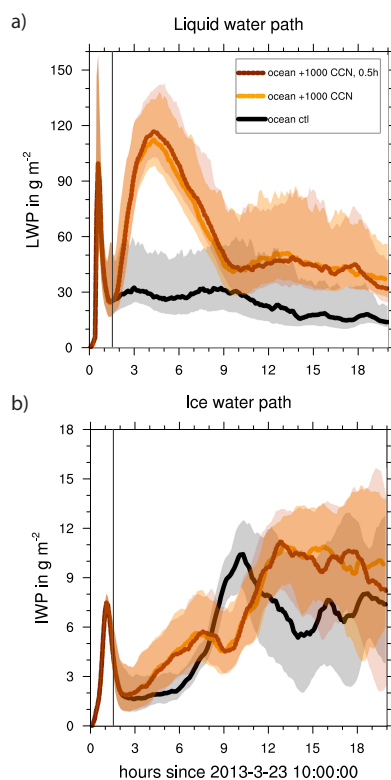
Figure 11. a) LWP and b) IWP over the open ocean in the *control* run, the *1000CCN*, and the *1000CCN_0.5h* simulations. The solid lines depict the median, the shading the interquartile ranges.

6   Discussion

A summary of our findings is shown in Fig. 12. The first panels conclude our findings from section 4, indicating the existence of two different cloud regimes, a stratocumulus and a homogeneous stratus regime over the open ocean and sea ice, respectively. These distinct regimes mainly result from differences in updraft speed, leading to differing efficiencies in cloud droplet growth,

5   precipitation and ice formation. Our results agree with previous findings obtained from satellites and measurement campaigns. As in Schweiger et al. (2008) we find a higher cloud base over the open ocean, accompanied with optically thicker clouds (supporting results by Palm et al., 2010). Similarly to Sotiropoulou et al. (2016) we also note structural differences over both surfaces with a stratocumulus cloud regime over the ocean versus a stratus cloud over sea ice. However, while Sotiropoulou et al. (2016) relate changes in cloud properties mainly to changes in atmospheric stability over the open ocean and sea ice, our

10   case studies are initialized with the same atmospheric stability profile (Fig. 1), hence we suggest that the differences in both regimes are primarily affected by surface fluxes.

In a next step, we applied aerosol perturbations to the two contrasting cloud regimes (Fig. 12, middle panels). Our results indicate a possible pathway for cloud-aerosol interactions in Arctic low-lying stratocumulus MPCs. As noted by others (e.g. Christensen et al., 2014; Possner et al., 2017) we also see an initial sensitivity of Arctic MPCs to aerosol perturbations. In our

15   simulations N_{drop} (R_{drop}) increases (decreases), accompanied by an increase in LWP. The thicker cloud increases τ and in addition triggers enhanced LW cooling at cloud top. We suggest that cloud top cooling poses a fundamental key to the feedback of CCN perturbations on the ice phase. The ice mass significantly increases through growth by deposition, additionally the increased N_{ice} as a result of immersion freezing at cloud top (as noted earlier by Possner et al., 2017) can contribute to an overall higher IWC in simulations solely perturbed by CCN.

20   Concerning the time scales of the initial perturbation response we find that the injection-to-peak time scale depends on the cloud regime. When updrafts are lower and the moisture flux is limited, as it is the case in our simulations over sea ice the response time is delayed by a factor of 2.5 compared to the open ocean where moisture is efficiently transported into the cloud layer by convective cloud structures (Fig. 6). Our main finding is that independent of the cloud regime, the environmental conditions, or the aerosol injection period, every perturbed cloud relaxes back to its unperturbed state. This relaxation time

25   scale is by a factor of 2 slower than the injection-to-peak time scale over the ocean and approximately equal to the injection-to-peak time over sea ice. In both regimes the perturbed simulations approximate their unperturbed state after 10-15 h simulation time.

To summarize the cloud microphysical properties of the sensitivity simulations during the polluted as well as the unpolluted period (as indicated by the arrows in Fig. 6), we calculated the mean cloud properties in Table 3. During the polluted period,

30   cloud-mean N_{drop} and LWP are increased, increasing τ. Note that over the full polluted period we do not find significant differences in cloud-mean N_{ice} and IWP. However, during the first 8 h (which is shorter than the full polluted time scale) we do see an increase in N_{ice} (Figure S4). In the post-polluted period, N_{drop}, LWP and τ remain slightly elevated compared to their unperturbed values, but are significantly decreased compared to the polluted period (Fig. 12, third panel).

	ocean_control	ocean_1000CCN	ice_control	ice_1000CCN
τ				
Polluted	2.82±0.23	8.70±3.49	2.58±0.40	10.88±4.33
Post-polluted	1.74±0.22	4.91±0.35	1.95±0.38	3.04±0.36
LWP $(\mathrm{g\,m^{-2}})$				
Polluted	28.65±2.48	71.54±25.52	25.50±2.73	85.92±37.74
Post-polluted	17.58±2.35	43.92±4.23	20.98±3.28	27.22±5.83
IWP $(\mathrm{g\,m^{-2}})$				
Polluted	4.80±3.20	4.68±1.85	2.84±1.32	4.71±4.53
Post-polluted	6.88±0.79	10.20±0.46	5.50±2.64	1.69±0.75
$N_{drop}(\mathrm{cm^{-3}})$				
Polluted	3.25±0.28	44.17±40.33	3.21±0.41	64.59±30.36
Post-polluted	3.32±0.38	19.78±4.86	3.66±0.30	9.31±2.63
$R_{drop}(\mu\mathrm{m})$				
Polluted	11.89±0.20	7.77±2.0	11.0±0.27	6.38±1.86
Post-polluted	11.70±0.47	8.78±0.43	10.78±0.18	9.42±0.94
$N_{ice}(\mathrm{L^{-1}})$				
Polluted	0.12±0.07	0.12±0.04	0.05±0.02	0.10±0.09
Post-polluted	0.24±0.02	0.30±0.03	0.09±0.02	0.04±0.01
R_{ice} $(\mu\mathrm{m})$				
Polluted	15.45±0.39	15.50±0.15	17.14±0.36	16.54±0.39
Post-polluted	13.61±0.25	14.17±0.58	16.87±0.34	16.54±0.31

Table 3. Mean cloud properties and standard deviation during the polluted (hour 2-12 over ocean and 3-14 over sea ice) and post-polluted period (hour 12-20/14-20), as indicated by the arrows in Fig. 6.

The absence of a long-term response in cloud properties to soluble aerosol perturbations ranging from 100-1000 $\mathrm{cm^{-3}}$ in magnitude is attributed to the efficient transport of aerosols out of the boundary layer. The accumulation of aerosols above the cloud has also been seen in independent WRF simulations of a different case recently published by Solomon et al. (2018). Therefore this mechanism has been seen across models and cases and deserves further investigation.

5   Nevertheless, we note that our study has come caveats. Due to runtime limitations it was not possible to simulate for a longer time period for these high-resolution simulations. Thus, we unfortunately cannot draw any conclusions concerning cloud persistence beyond 20 h.
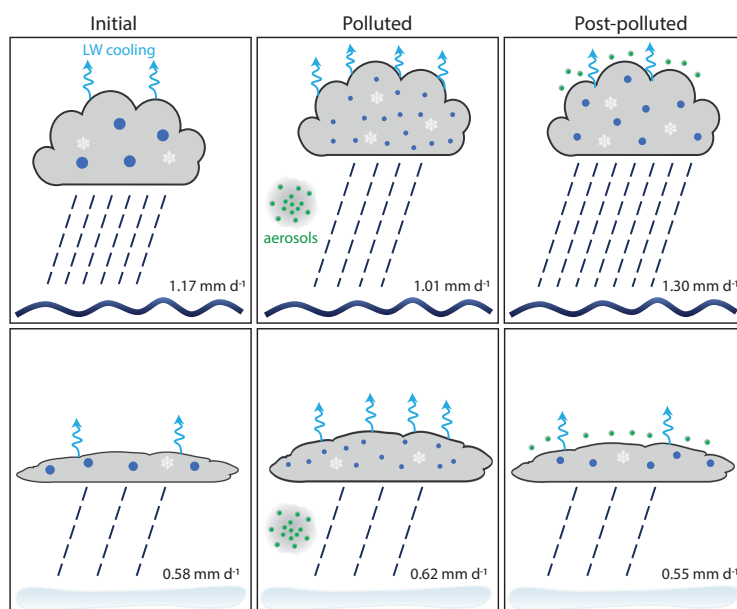
Figure 12. Conceptual overview of the aerosol response in the initial (unpolluted), polluted and post-polluted state. The first row illustrates the open ocean stratocumulus regime, the lower row the stratus sea ice regime.

7 Conclusions

The analysis of MPCs within a changing Arctic environment has been the subject of a number of recent studies. Here, we addressed in a series of high resolution LES the cloud properties of a MPC in two differing regimes (i.e. sea ice and open ocean) and performed several aerosol perturbation experiments, contrasting our results in both regimes. The robustness of the response to an aerosol perturbation was evaluated by applying our perturbation scenarios in warmer/colder environmental conditions and by changing the aerosol injection period.

Our key findings are summarized as follows:

1. The surface properties have a significant impact on MPC properties. Over the open ocean, strong turbulent surface fluxes increase the updraft velocities, which in turn favor the development of cumuli towers feeding moisture into the stratus layer. This increased vertical moisture flux leads to an increase in the cloud LWC. Over sea ice, surface fluxes and in turn updraft velocities are low, which leads to limited cloud droplet growth and a rather thin stratus cloud which is confined to a few hundred meters below the capping inversion. Ice formation is less efficient than over the open ocean. As a result of lower LWC and IWC, τ is lower over sea ice than over the open ocean, implying differences in the cloud radiative forcing between the two regimes.

2. Aerosol perturbations resembling potential CCN significantly impact the cloud LWC and IWC immediately after the perturbation injection. The MPC over the ocean responds with an increase in N_{drop} and LWC. Through increased LW cooling, ice crystals form below cloud top by immersion freezing and subsequently grow by deposition, which increases the IWC. Over sea ice, cloud droplet growth is less efficient and the maximum response is delayed from 2.5 h over the open ocean to 7 h over sea ice in the most perturbed simulation.

   INP perturbations immediately increase the IWC and decrease the LWC in both cloud regimes, however, none of the applied INP perturbations (3 and 10 L^{-1}) leads to a complete cloud glaciation.

3. Vertical mixing of additional aerosols out of the boundary layer results in an attenuated CCN response after 10-15 h. The cloud system returns to its unperturbed state and cloud properties relax to values close to the variability of the control simulation. This response is delayed over sea ice, but robust between both regimes.

4. Finally, we demonstrate the response to aerosol perturbations being consistent among different temperature regimes and aerosol injection periods.

Our simulations provide evidence of a possible pathway for aerosol-cloud interactions considering the effect of aerosol processing in the Arctic. Nevertheless, as previously mentioned we note that the vertical transport of soluble aerosol from the boundary layer above the inversion may be too efficient in our simulations which leads to an underestimate of N_{drop}. However, sufficient CCN still remain in the boundary layer and the strength of available CCN varies with injection strength of soluble aerosol. Therefore, while the mechanism may be too efficient in these simulations, we still are able to make a robust assessment of cloud sensitivity to aerosol perturbations. Given that this mechanism was also seen in independent simulations

for a different case of MPCs, in different environmental conditions, performed with a different model, we argue that it deserves further investigation. Additional observations of vertical cloud and aerosol profiles from upcoming Arctic field campaigns could help to constrain such a CCN transport mechanism.

Author contributions. GE conducted the simulations, analysed the results, and was the main author of the paper. AP and UL contributed to
5   the design of the study and the analysis of the results. All authors contributed to the writing of the study.

Acknowledgements. The research leading to these results has received funding from the European Union's Seventh Framework Program (FP7/2007-2013) project BACCHUS under grant agreement No 603445. All simulations were performed with the Consortium for Small-scale Modeling (COSMO) model adapted for large eddy simulations. The simulations were performed and are stored at the Swiss National Supercomputing Center (CSCS). The ACCACIA observations were obtained from the NCAS British Atmospheric Data Center
10   (http://catalogue.ceda.ac.uk/uuid/88f95b1d52804b27882fbb798b116d3a).

References

Bennartz, R., Shupe, M. D., Turner, D. D., Walden, V. P., Steffen, K., Cox, C. J., Kulie, M. S., Miller, N. B., and Pettersen, C.: July 2012 Greenland melt extent enhanced by low-level liquid clouds., Nature, 496, 83–6, doi:10.1038/nature12002, 2013.

Berner, A. H., Bretherton, C. S., and Wood, R.: Large eddy simulation of ship tracks in the collapsed marine boundary layer: A case study from the Monterey area ship track experiment, Atmospheric Chemistry and Physics, 15, 5851–5871, doi:10.5194/acp-15-5851-2015, 2015.

Browse, J., Carslaw, K. S., Mann, G. W., , et al.: The complex response of Arctic aerosol to sea-ice retreat, Atmos. Chem. Phys., 14, 7543–7557, doi:10.5194/acp-14-7543-2014, 2014.

Christensen, M. W., Suzuki, K., Zambri, B., and Stephens, G.: Ship track observations of a reduced shortwave aerosol indirect effect in mixed-phase clouds, Geophys. Res. Lett., 41, 6970–6977, doi:10.1002/2014GL061320, 2014.

Cohen, J., Screen, J. A., Furtado, J. C., Barlow, M., Whittleston, D., Coumou, D., Francis, J., Dethloff, K., Entekhabi, D., Overland, J., and Jones, J.: Recent Arctic amplification and extreme mid-latitude weather, Nat. Geosci., 7, 627–637, doi:10.1038/ngeo2234, 2014.

Curry, J. A., Rossow, W. B., Randall, D., and Schramm, J.: Overview of Arctic Cloud and Radiation Characteristics, J.Climate, 9, 1731–1764, 1996.

DeMott, P. J., Prenni, A. J., McMeeking, G. R., and Others, A.: Integrating laboratory and field data to quantify the immersion freezing ice nucleation activity of mineral dust particles, Atmospheric Chemistry and Physics, 15, 393–409, doi:10.5194/acp-15-393-2015, 2015.

Garrett, T. J. and Zhao, C.: Increased Arctic cloud longwave emissivity associated with pollution from mid-latitudes, Nature, 440, 787–789, doi:10.1038/nature04636, 2006.

Gilgen, A., Ting Katty Huang, W., Ickes, L., Neubauer, D., and Lohmann, U.: How important are future marine and shipping aerosol emissions in a warming Arctic summer and autumn?, Atmos. Chem. Phys., 18, 10 521–10 555, doi:10.5194/acp-18-10521-2018, 2018.

IPCC: Summary for Policymakers., in: Climate Change 2013: The Physical Science Basis. Contribution of Working Group 1 to the Fifth Assessment Report of the Intergovernmental Panel on Climate Change., 2013.

Jackson, R. C., McFarquhar, G. M., Korolev, A. V., , et al.: The dependence of ice microphysics on aerosol concentration in arctic mixed-phase stratus clouds during ISDAC and M-PACE, J. Geophys. Res., 117, 1–20, doi:10.1029/2012JD017668, 2012.

Khon, V. C., Mokhov, I. I., Latif, M., , et al.: Perspectives of Northern Sea Route and Northwest Passage in the twenty-first century, Climatic Change, 100, 757–768, doi:10.1007/s10584-009-9683-2, 2010.

Liu, Y., Key, J. R., Liu, Z., Wang, X., and Vavrus, S. J.: A cloudier Arctic expected with diminishing sea ice, Geophys. Res. Lett., 39, 1–5, doi:10.1029/2012GL051251, 2012.

Lloyd, G., Choularton, T. W., Bower, K. N., , et al.: Observations and comparisons of cloud microphysical properties in spring and summertime Arctic stratocumulus clouds during the ACCACIA campaign, Atmos. Chem. Phys., 15, 3719–3737, doi:10.5194/acp-15-3719-2015, 2015.

Loewe, K., Ekman, A. M. L., Paukert, M., Sedlar, J., Tjernström, M., and Hoose, C.: Modelling micro- and macrophysical contributors to the dissipation of an Arctic mixed-phase cloud during the Arctic Summer Cloud Ocean Study (ASCOS), Atmos. Chem. Phys., 17, 6693–6704, doi:10.5194/acp-2016-917, 2017.

Lohmann, U., Henneberger, J., and Henneberg, O.: Persistence of orographic mixed-phase clouds, Geophys. Res. Lett., pp. 1–8, doi:10.1002/2016GL071036, 2016.

Mauritsen, T., Sedlar, J., Tjernström, M., and Others, A.: An Arctic CCN-limited cloud-aerosol regime, Atmos. Chem. Phys., 11, 165–173, doi:10.5194/acp-11-165-2011, 2011.

Miltenberger, A. K., Field, P. R., Hill, A. A., Rosenberg, P., Shipway, B. J., Wilkinson, J. M., Scovell, R., and Blyth, A. M.: Aerosol-cloud interactions in mixed-phase convective clouds. Part 1: Aerosol perturbations, Atmos. Chem. Phys., 18, 10 593–10 613, doi:10.5194/acp-2017-788, 2018.

Mironov, D., Ritter, B., Schulz, J. P., Buchhold, M., Lange, M., and Machulskaya, E.: Parameterisation of sea and lake ice in numerical weather prediction models of the German Weather Service, Tellus, Series A: Dynamic Meteorology and Oceanography, 64, 1–16, doi:10.3402/tellusa.v64i0.17330, 2012.

Morrison, H., de Boer, G., Feingold, G., , et al.: Resilience of persistent Arctic mixed-phase clouds, Nat. Geosci., 5, 11–17, doi:10.1038/ngeo1332, 2011.

Nenes, A. and Seinfeld, J. H.: Parameterization of cloud droplet formation in global climate models, Journal of Geophysical Research: Atmospheres, 108, 4415, doi:10.1029/2002JD002911, 2003.

Overland, J. E. and Wang, M.: When will the summer Arctic be nearly sea ice free ?, Geophys. Res. Lett., 40, 2097–2101, doi:10.1002/grl.50316, 2013.

Palm, S. P., Strey, S. T., Spinhirne, J., and Markus, T.: Influence of Arctic sea ice extent on polar cloud fraction and vertical structure and implications for regional climate, J. Geophys. Res., 115, 1–9, doi:10.1029/2010JD013900, 2010.

Peters, G. P., Nilssen, T. B., Lindholt, L., Eide, M. S., Glomsrod, S., Eide, L. I., and Fuglestvedt, J. S.: Future emissions from shipping and petroleum activities in the Arctic, Atmos. Chem. Phys., 11, 5305–5320, doi:10.5194/acp-11-5305-2011, 2011.

Possner, A., Ekman, A. M., and Lohmann, U.: Cloud response and feedback processes in stratiform mixed-phase clouds perturbed by ship exhaust, Geophys. Res. Lett., 44, 1964–1972, doi:10.1002/2016GL071358, 2017.

Ralph, F. M., Neiman, P. J., and Rotunno, R.: Dropsonde Observations in Low-Level Jets over the Northeastern Pacific Ocean from CALJET-1998 and PACJET-2001 : Mean Vertical-Profile and Atmospheric-River Characteristics, Mon. Wea. Rev.,, 133, 889–910, 2005.

Ritter, B. and Geleyn, J.-F.: A Comprehensive Radiation Scheme for Numerical Weather Prediction Models with Potential Applications in Climate Simulations, doi:10.1175/1520-0493(1992)120<0303:ACRSFN>2.0.CO;2, 1992.

Schättler, U., Doms, G., and Steppele, J.: Requirements and problems in parallel model development at DWD., Scientific Programming, 8, 13–22, 2000.

Schweiger, A. J., Lindsay, R. W., Vavrus, S., and Francis, J. A.: Relationships between Arctic sea ice and clouds during autumn, J.Climate, 21, 4799–4810, doi:10.1175/2008JCLI2156.1, 2008.

Sedlar, J., Shupe, M. D., and Tjernström, M.: On the relationship between thermodynamic structure and cloud top, and its climate significance in the Arctic, J.Climate, 25, 2374–2393, doi:10.1175/JCLI-D-11-00186.1, 2012.

Seifert, A. and Beheng, K. D.: A two-moment cloud microphysics parameterization for mixed-phase clouds. Part 1: Model description, Meteor. Atm. Phys., 92, 45–66, doi:10.1007/s00703-005-0112-4, 2006.

Seifert, A., Heus, T., Pincus, R., and Stevens, B.: Large-eddy simulation of the transient and near-equilibrium behavior of precipitating shallow convection, J. Adv. Model. Earth Syst., 7, 1918–1937, doi:10.1002/2015MS000510.Received, 2015.

Serreze, M. C. and Barry, R. G.: Processes and impacts of Arctic amplification: A research synthesis, Global Planet. Change, 77, 85–96, doi:10.1016/j.gloplacha.2011.03.004, 2011.

Shupe, M. D., Matrosov, S. Y., and Uttal, T.: Arctic Mixed-Phase Cloud Properties Derived from Surface-Based Sensors at SHEBA, J. Atmos. Sci., 63, 697–711, doi:10.1175/JAS3659.1, 2006.

Shupe, M. D., Walden, V. P., Eloranta, E., , et al.: Clouds at Arctic atmospheric observatories. Part I: Occurrence and macrophysical proper-
ties, J. Appl. Meteor. Climatol., 50, 626–644, doi:10.1175/2010JAMC2467.1, 2011.

Solomon, A., Feingold, G., and Shupe, M. D.: The role of ice nuclei recycling in the maintenance of cloud ice in Arctic mixed-phase
stratocumulus, Atmos. Chem. Phys., 15, 10 631–10 643, doi:10.5194/acp-15-10631-2015, 2015.

5   Solomon, A., de Boer, G., Creamean, J. M., McComiskey, A., Shupe, M. D., Maahn, M., and Cox, C.: The relative impact of cloud con-
densation nuclei and ice nucleating particle concentrations on phase-partitioning in Arctic Mixed-Phase Stratocumulus Clouds, Atmos.
Chem. Phys. Discuss., pp. 1–33, doi:10.5194/acp-2018-714, 2018.

Sotiropoulou, G., Tjernstrom, M., Sedlar, J., Achtert, P., Brooks, B. J., Brooks, I. M., Perssond, P. O. G., Prytherch, J., Salisbury, D. J., Shuped,
M. D., Johnstond, P. E., and Wolfe, D.: Atmospheric conditions during the arctic clouds in summer experiment (ACSE): Contrasting open
10   water and sea ice surfaces during melt and freeze-up seasons, J.Climate, 29, 8721–8744, doi:10.1175/JCLI-D-16-0211.1, 2016.

Stevens, B. and Feingold, G.: Untangling aerosol effects on clouds and precipitation in a buffered system., Nature, 461, 607–613,
doi:10.1038/nature08281, 2009.

Stevens, R. G., Loewe, K., Dearden, C., Dimitrelos, A., Possner, A., Eirund, G. K., Raatikainen, T., Hill, A. A., Shipway, B. J., Wilkinson,
J., Romakkaniemi, S., Tonttila, J., Laaksonen, A., Korhonen, H., Connolly, P., Lohmann, U., Hoose, C., Ekman, A. M. L., Carslaw, K. S.,
15   and Field, P. R.: A Model Intercomparison of CCN-Limited Tenuous Clouds in the High Arctic, Atmos. Chem. Phys., 18, 11 041–11 071,
doi:10.5194/acp-2017-1128, 2018.

Struthers, H., Ekman, A. M. L., Glantz, P., , et al.: The effect of sea ice loss on sea salt aerosol concentrations and the radiative balance in the
Arctic, Atmos. Chem. Phys., 11, 3459–3477, doi:10.5194/acp-11-3459-2011, 2011.

Tan, I., Storelvmo, T., and Zelinka, M.: Observational constraints on mixed-phase clouds imply higher climate sensitivity, Science, 352,
20   224–227, 2016.

Tjernström, M., Leck, C., Birch, C. E., , et al.: The Arctic Summer Cloud Ocean Study (ASCOS): Overview and experimental design, Atmos.
Chem. Phys., 14, 2823–2869, doi:10.5194/acp-14-2823-2014, 2014.

Twomey, S.: Pollution and the Planetary Albedo, Atmos. Environ., 8, 1251–1256, doi:10.1016/j.atmosenv.2007.10.062, 1974.

Van Tricht, K., Lhermitte, S., Lenaerts, J. T., Gorodetskaya, I. V., L'Ecuyer, T. S., Noël, B., Van Den Broeke, M. R., Turner, D. D., and Van
25   Lipzig, N. P.: Clouds enhance Greenland ice sheet meltwater runoff, Nat. Commun., 7, 1–9, doi:10.1038/ncomms10266, 2016.

Vavrus, S., Holland, M. M., and Bailey, D. A.: Changes in Arctic clouds during intervals of rapid sea ice loss, Clim. Dyn., 36, 1475–1489,
doi:10.1007/s00382-010-0816-0, 2010.

Ye, K., Jung, T., and Semmler, T.: The influences of the Arctic troposphere on the midlatitude climate variability and the recent Eurasian
cooling, Journal of Geophysical Research: Atmospheres, doi:10.1029/2018JD028980, 2018.

30   Young, G., Jones, H. M., Choularton, T. W., , et al.: Observed microphysical changes in Arctic mixed-phase clouds when transitioning from
sea ice to open ocean, Atmos. Chem. Phys., 16, 13 945–13 967, doi:10.5194/acp-2016-409, 2016.

Young, G., Connolly, P. J., Dearden, C., and Choularton, T. W.: Large-scale subsidence promotes convection in sub-Arctic mixed-phase
stratocumulus via enhanced below-cloud rain evaporation, Atmos. Chem. Phys., pp. 1–33, 2017a.

Young, G., Connolly, P. J., Jones, H. M., and Choularton, T. W.: Microphysical sensitivity of coupled springtime Arctic stratocumulus to
35   modelled primary ice over the ice pack, marginal ice, and ocean, Atmos. Chem. Phys., 17, 4209–4227, doi:10.5194/acp-17-4209-2017,
2017b.